Environ. Sci. Technol. **2006**, *40,* 1609−1615

UV Reactor Performance Modeling by Eulerian and Lagrangian Methods

D. ANGELO SOZZI AND FARIBORZ TAGHIPOUR*

Department of Chemical and Biological Engineering, University of British Columbia, 2360 East Mall, Vancouver, British Columbia, V6T 1Z3, Canada

A study was performed to investigate the influence of hydrodynamics on the performance of ultraviolet (UV) reactors. Two general UV disinfection models were developed by integrating fluence rate models and inactivation kinetics within a commercial computational fluid dynamics (CFD) software package to predict reactor performances. Both a particle tracking (Lagrangian) random walk model and a volumetric reaction rate based (Eulerian) model were implemented. Simulations were performed for two characteristic annular single-lamp UV reactor configurations, with inlets concentric (L-shape) and normal (U-shape) to the reactor axis. Two fluence rate models, the infinite line source assumption and the finite line or multiple point source summation (MPSS), were used. First-order inactivation kinetics was assumed for disinfection, with rate constants from MS2 bacteriophage assays. The simulation results provided detailed information on the velocity profiles, reaction rates, range of absorbed dose, and areas of short circuiting of the UV reactors. Model predictions based on both the Lagrangian dose distribution and Eulerian concentration distribution were in good agreement with each other at high flow rates but showed some discrepancies at lower flow rates. Experimental verification of the general models was performed by simulating the disinfection performance of an industrial prototype UV reactor. Results from both integration approaches were shown to be in good agreement with the provided biodosimetry data.

1 Introduction

Alternative water treatment methods have gained popularity because of increasingly stringent environmental regulations and concerns regarding chemical treatment methods. UV-based technologies, especially, have seen a rapid growth over the past decade (*1*). The use of UV radiation for disinfection relies on the inactivation of microorganisms through changes in the pathogens' DNA (i.e., formation of thymine dimers), rendering them unable to reproduce. UV application for advanced oxidation processes (AOPs) involves exciting a strong oxidant such as H_2O_2 or O_3 to generate highly reactive hydroxyl radicals to oxidize (toxic) organic substrates. In both applications, the local rate of reaction is linked to the nonuniform radiation distribution (UV-fluence rate). Reactor performance is thus strongly dependent on hydrodynamic transport processes, influencing the spatial distribution of the microorganisms or toxic substrates. The influence of the flow field and reactor geometry on the performance of disinfection systems has been demonstrated by Schoenen et al. (*2*) and Chiu et al. (*3*), while the effect of interactions between reactor hydrodynamics and local radiation fluence on contaminants in AOPs was shown by Pareek et al. (*4*).

In a UV reactor, the fluid behavior defines the spatial concentration distribution and flow of chemical agents or microorganisms through the reactor volume. UV lamp(s) supply the radiation driving the main reaction, with fluence rate attenuated by the distance from the lamp and transmittance of the media. Finally, the reaction rate is determined by the local UV- fluence rate, concentration of the species, and the kinetic rate constants. Modeling photoreactors therefore involves three submodels for hydrodynamics, radiation fluence rate distribution, and UV-reaction kinetics that are coupled by the material and energy balances.

The use of advanced numerical simulation tools, in particular computational fluid dynamics (CFD), to model the flow and transport in chemical engineering processes has attracted much attention in recent years (e.g., *4*−*6*). Integrated CFD models have also been used to simulate photoreactor performance (e.g., *3, 7, 8*). A key advantage of simulating reactor performance by solving the governing equations of the system is the virtual prototyping capability, allowing cutting of costs by reducing design cycle times and evaluating more design alternatives than practical in the past (*9, 10*).

The objective of this work was to implement an integrated numerical model to evaluate the performance of UV-disinfection reactors. UV-radiation models and (volumetric) reaction rate models were developed and coupled with a commercial CFD code, Fluent 6.2, that provided the necessary code extensions to implement and execute the submodels. Annular UV reactors with a concentric lamp parallel to the reactor axis, representing a widely used design for UV reactors, were investigated. Both, continuum (Eulerian) and dispersed phase (Lagrangian) approaches to disinfection modeling were implemented, combining a spatial UV-fluence rate model with first-order kinetics for disinfection. The effect of UV-radiation models on reactor performance was studied by considering infinite line source and finite line source models. The numerical disinfection efficiency (log reduction) for two reactor geometries, inlet normal to the reactor axis (U-shape) and inlet parallel to the reactor axis (L-shape), were compared for several flow rates. The performance of a commercially available annular UV reactor was then simulated based on the technical data and biodosimetry results.

2 Modeling Setup

2.1 Flow Model. Two annular reactor geometries with different inlet positions (L- and U-shape) but similar dimensions (Table 1) were used in this study (Figure 1a and b). The reactors contained an annular UV lamp and inlet/outlet ports located 3.81 cm (1.5 in.) from either end for the U-shape reactor, or with the inlet concentric on the front-plate for the L-shape reactor. A third industrial prototype UV reactor, designed by R-Can Environmental Inc., provided the basis for the comparison of model predictions to the biodosimetry results. This L-shape design contained a larger lamp holder and an additional baffle close to the outlet, both of which were accounted for (Figure 1c).

Reynolds Averaged Navier Stokes (RANS) equations, derived from the general steady-state form of the governing equations for the conservation of mass

$$\nabla\cdot(\rho\vec{v}) = 0 \qquad (1)$$

* Corresponding author tel:+1-604-822-1902; fax: +1-604-822-5407; e-mail: fariborz@chml.ubc.ca.

10.1021/es051006x CCC: $33.50
Published on Web 01/21/2006

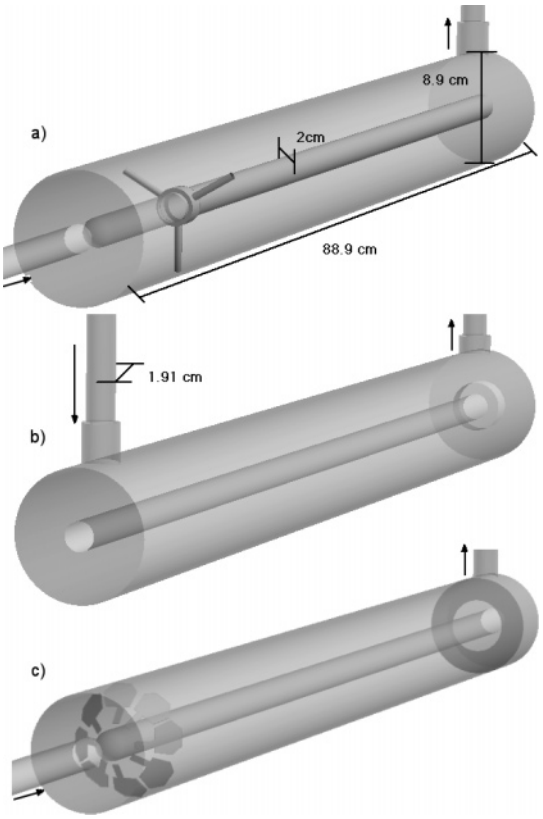

FIGURE 1. Reactor geometries of (a) L-shape with lamp holder, (b) U-shape, and (c) industrial prototype (L-shape with lamp holder).

TABLE 1. Dimensons for the L-Shape, U-Shape, and Industrial Prototype (L-Shape) Reactor Geometries

	U-shape and L-shape	prototype
reactor body		
diameter	8.9 cm (3.5 in.)	8.6 cm
length	88.9 cm (35 in.)	101 cm
lamp		
diameter	2 cm	2.26 cm
arc length	80 cm	88 cm
UV output	35 W	35 W
inlet/outlet		
diameter	1.91 cm (0.75 in.)	2.24 cm
length	85 cm (34 in.)	100 cm

and the conservation of momentum,

$$\nabla\cdot(\rho\,\vec{v}\,\vec{v}) = -\nabla P + \nabla\cdot(\bar{\tau}) + \rho g \qquad (2)$$

where ρ is density, $\vec{v}$ is velocity, P is pressure, $\bar{\tau}$ is the stress tensor, and g is the gravitational acceleration, were solved using a finite volume based commercial CFD software package (Fluent 6.2). In RANS simulations, the time-averaged momentum transport equations are closed by modeling the momentum flux terms (Reynolds stresses) using a turbulence model. In this work, the realizable κ-ϵ turbulence model was used. To simulate the reactor hydrodynamics using CFD, the domains were discretized using a mix of structured and unstructured meshes (0.5−1 million cells). No-slip boundary conditions were set at the reactor walls and the UV lamp. The inlet boundary conditions were defined as a mass flow with the fluid properties of liquid water and 10% turbulent intensity over the diameter. An inlet tube with an $L_1/D_1 = 45$ ensured a fully developed flow entering the reactor. Numerical convergence was defined at scaled residuals smaller than 1×10^{-5} for second order upwind solutions. Computations were carried out on a Pentium 4 1.8 GHz CPU, with 1 GB of memory and second order convergence was typically reached after 12−16 h.

2.2 UV-Fluence Rate Models. Assuming uniform optical properties of the fluid, the UV-fluence rate at any given point can be described independent of the flow field, as a function of the distance to the source, the optical transmissivity of the fluid, and the initial UV output (*12*). The assumption implies low concentrations of contaminants and little or no change in the optical behavior of the reacting agent, which are appropriate for the case of UV disinfection. Monochromatic UV-fluence models of increasing complexity, from one-dimensional radial to discrete ordinate (DO), have been proposed (*13*). For the present study it was assumed that shadowing, reflection, and refraction effects have little influence on the final distribution. Two UV models describing the spatial distribution of fluence rate were implemented in the reactor performance model to calculate the fluence rate at each point as a function of its distance from the lamp and the UV transmittance of the medium.

2.2.1 Infinite Line Source or Radial Model. This model assumes the lamp to be represented as a line source with radiation emitted normal to the lamp axis. The fluence rate E, is related to the UV lamp radiant power per unit length and the radial distance, r [cm], from the lamp center line (*14*). Simplified for an axisymmetric annular system, the local fluence rate, $E(r)$, is expressed as

$$E(r) = \frac{\frac{P}{L_2}}{2\pi r} exp[\sigma_w(r - r_L)] \qquad (3)$$

where P is the total germicidal lamp output [mW], L_2 is the axial lamp arc length [cm], r_L is the lamp sleeve radius [cm], and σ_w is the absorption coefficient of the fluid [cm^{-1}]. σ_w can be calculated from the transimissivity, T, by the following equation

$$\sigma_w = ln(10)\log(T) \qquad (4)$$

This model does not deal with refraction or reflection and cannot describe what happens near the lamp ends, but it is easy to implement and has been shown to perform reasonably well for standard reactor sizes (*13*).

2.2.2 Finite Line Source or Multiple Point Source Summation (MPSS) Model. In this model the lamp is approximated as a series of point light sources emitting radiation in all directions (*12*). The UV-fluence at each location in the domain is estimated as the sum of energy received from each individual point source in the system:

$$E(r, z) = \sum_{i=1}^{n} \frac{\frac{P}{n}}{4\pi l_i^2} exp\left[-\sigma_w(r - r_L)\frac{l_i}{r}\right] \qquad (5)$$

where z [cm] represents the axial distance and l_i is the distance from the current location [cm] to the point source number n_i out of a total of n sources. Results were found to be independent of the number of sources with $n \geq 100$ for the present models. Fluence rate changes over the length of the lamp and diffuse radiation at the lamp ends are predicted with this model, but it has been suggested that the model overpredicts fluence rates close to the lamp surface (*13*).

2.3 Disinfection Kinetics Model. MS2 bacteriophage biodosimetry is one of the methods of choice for log inactivation studies of UV-disinfection systems and a standardized protocol is available from the USEPA Environmental Technology Verification (ETV) program. MS2 is nonpathogenic to humans, has a relatively high UV resistance, and,

being a single-stranded RNA virus, its dose response for UV inactivation can be described by conventional first-order Chick−Watson kinetics:

$$N = N_0 e^{-kEt} \tag{6}$$

where N_0 represents the initial organism concentration (plaque-forming units per mL)[PFU/mL] and N is the organism concentration after UV exposure [PFU/mL], k is the inactivation rate constant [cm^2/mJ], E is the UV-fluence rate [mW/cm^2], and t is the exposure time [s]. Dose (also referred to as fluence) is defined as the UV-fluence rate multiplied by the time, i.e., $D = E \times t$ [mJ/cm^2]. In general usage, the SI units are exchanged for the equivalent but more manageable units shown here (*15*).

Dose response curves are measured under tightly controlled conditions using a collimated beam of UV to eliminate the influence of hydrodynamics and nonuniform fluence rates, and are recorded as the log inactivation ($\log N_0/N$) per unit dose. The rate constant k in eq 6 can be obtained from the slope of [$\log (N_0/N)/\log(e)$] plotted against dose, D. Each culture of MS2 macrophages has to be calibrated separately, but an inactivation constant of $k = 0.1$ cm^2/mJ has been reported by several sources (*16*−*18*).

2.4 Integrated Reactor Performance Model. For disinfection reactions in continuous reactors, the path a microorganism takes is key to the amount of UV radiation (dose) it absorbs. The position of microorganisms in the reactor can be tracked in the Eulerian or Lagrangian reference frames.

2.4.1 Lagrangian Model. In the Lagrangian framework, after obtaining the velocity field by solving the transport equations, organisms are treated as discrete particles where the trajectory is predicted by integrating the force balance on the particle. Random effects of turbulence on the particle are accounted for by the discrete random walk (DRW), or "eddy lifetime" model, where the interaction of a particle with a succession of discrete stylized fluid phase turbulent eddies is simulated (*19*). The particle trajectories are computed based on a steady continuous-phase flow field. A statistically significant number of particles (representing microorganisms) is released at the reactor inlet (N_0) and the absorbed dose is integrated along the path of each particle. The absorbed dose at each point is calculated by multiplying the average local fluence rate (E) by the time period Δt that the particle is exposed to that certain local fluence rate. For each dose interval i, the number of microorganisms that remain vital, N_i, is calculated by

$$N_i = \alpha_i \times N_0 e^{-kD_i} \tag{7}$$

where α_i is the fraction of particles that receive the dose D_i, k is the inactivation rate constant, and D_i is the average dose for the ith bin interval. The sum of all vital particles over the entire range of doses yields the estimated total number of vital particles (microorganisms) leaving the reactor, N:

$$N = \sum N_i \tag{8}$$

2.4.2 Eulerian Model. In the Eulerian framework, the conservation equation of species (microorganisms) is solved along with the transport equations. The local mass fraction of each species is predicted through the convective-diffusion equation for the species to calculate the concentration of living bacteria through the domain

$$\nabla\cdot(\vec{v}C) = -\nabla\cdot\vec{J} + R \tag{9}$$

where $\vec{J}$ and R are the diffusion flux (including turbulent dispersion) of the species and the source (reaction) rate,

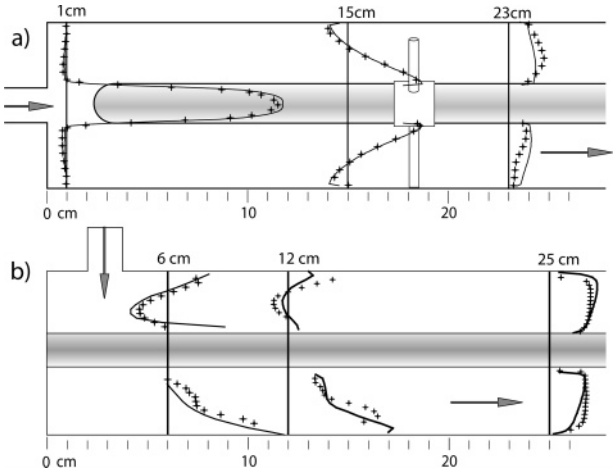

FIGURE 2. Comparison of axial flow velocity data (+) from particle image velocimetry (PIV) to CFD simulations (lines). Measurements are illustrated at key positions along the central plane of (a) L-shape (with annular UV lamp and lamp holder) and (b) U-shape (with annular UV lamp) reactors. Vertical lines indicate both position and axial velocity zero of the measurements. The maximum velocities (m/s) at the various positions (cm) from the reactor inlets are as follows: 2.8 m/s at 1 cm, 1.8 m/s at 15 cm, 0.8 m/s at 23 cm in reactor (a) and 0.5 m/s for all positions in reactor (b).

respectively. For microorganisms with linear inactivation rate and rate constant k, the rate of inactivation R is defined as

$$R = -kEC \tag{10}$$

where E is the local fluence rate and C is the microorganism concentration. For the RANS equation of species conservation, the eddy dissipation model was used to solve the transport equations of the species (*20*). After discretization of the reactor domain into small cells, volumetric reaction rates are calculated based on the local fluence rate and microorganism concentration for each cell (*21*). Each cell is thus treated as a completely mixed reactor with locally uniform microbial concentration, UV fluence, and a reaction rate defined by eq 10.

3 Experimental Section

A stock solution of MS2 (*E. coli* bacteriophage ATCC 15597-B1) was prepared, according to the ISO 10705-1 protocol, using an *E. coli* host (*E. coli* ATCC 15597). MS2 was added to the feed tank in a concentration of 1×10^6 PFU/mL. Samples of 50 mL were taken at the reactor inlet and outlet after steady state was reached.

The MS2 coliphages were enumerated using a standard overlay agar assay method (standard method 9211-D (*22*)). The frozen *E. coli* host was thawed in a water bath, one tube per sample. A 1-mL portion of *E. coli* was added to 5 mL of sample and 6 mL of modified trypticase soy agar (MTSA) and mixed thoroughly. The broth was then poured into Petri dishes containing TSA. The agar was allowed to solidify in the covered dishes. The plates were then inverted and incubated at 35 °C overnight. The plaques were counted, multiplied by the dilution factor, and divided by the sample volume in milliliters to obtain the titer in PFU/mL.

4 Results and Discussion

4.1 Flow Field. The CFD models describing the flow and the choice of turbulence model on the hydrodynamic flow field in annular reactors were evaluated by comparing the predicted results with those obtained experimentally using particle image velocimetry (PIV), the details of which are discussed elsewhere (*11*). The results demonstrated close agreements between modeling and experimental data (Figure

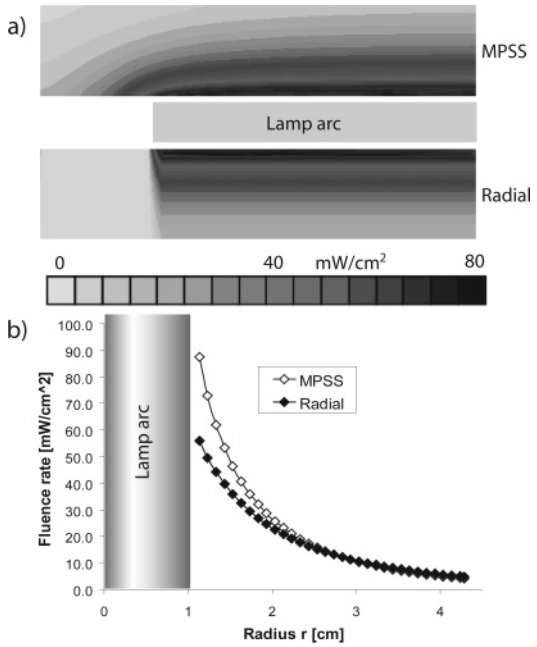

FIGURE 3. (a) Fluence rate distribution at the lamp ends for the radial and MPSS radiation models. (b) Fluence rates from lamp surface to reactor walls for both radiation models, at the center of the lamp arc.

2), indicating the accuracy of the hydrodynamic models in predicting reactor flow fields.

4.2 Fluence Rate. Figure 3a shows a two-dimensional representation of the UV-fluence rates in the annular reactor as calculated by the MPSS and radial radiation models for a germicidal UV output of 35 W over the 80-cm lamp arc at a UV transmissivity of 70% (per cm) for the fluid. The contours of fluence at the lamp ends clearly illustrate the differences between the two modeling approaches. UV-fluence rates from the reactor walls to the lamp surface ranged from 8 to 100 mJ/cm^2 for the MPSS and from 5 to 60 mJ/cm^2 for the radial model. The radial profiles (Figure 3b) show that the MPSS model predicts higher fluence rates than the radial model close to the lamp surface; this corresponds to the model limitations described by Blatchley (*12*). Both models predict reasonable values at distances of 2.5 cm and more from the lamp and show good agreement with experimental UV-fluence rate measurements on the basis of actinometry (*13*). Closer to the UV source where the models show the greatest deviation from each other, however, experimental measurements for model evaluation are hard to obtain because of physical limitations (the radius of the actinometry spheres is too large). In the UV reactor configuration under study, with a lamp radius of 1 cm and a tube radius of 4.45 cm, much of the reactor volume lies within the zone where the MPSS model predicts a higher fluence rate than the radial model.

4.3 Lagrangian Approach for Simulating Reactor Performance. The dose distributions for an annular L-shape reactor with a flow rate of 25 GPM was estimated based on the Lagrangian tracking of microorganisms as described earlier. Figure 4 shows particle trajectories calculated by the random walk model, colored by the absorbed dose. Consistent results were found by releasing 10 000 or more particles in batches of 500 uniformly distributed over the reactor inlet. The doses received by the microorganisms were in the range of 21−270 mJ/cm^2 with an average of 68 mJ/cm^2 (Figure 5). Short circuiting, where microorganisms predominantly pass quickly through regions of lower fluence rate, does not occur (no peak at lower doses), but the wide-spread and nonuniform dose distribution shows that the hydrodynamic efficiency can be improved. Better mixing throughout the domain might lead to a narrower dose distribution and thus more efficient use of the radiation energy. A log reduction of 1.87 was calculated from the dose distribution for a disinfection rate constant of $k = 0.1$ cm^2/mJ.

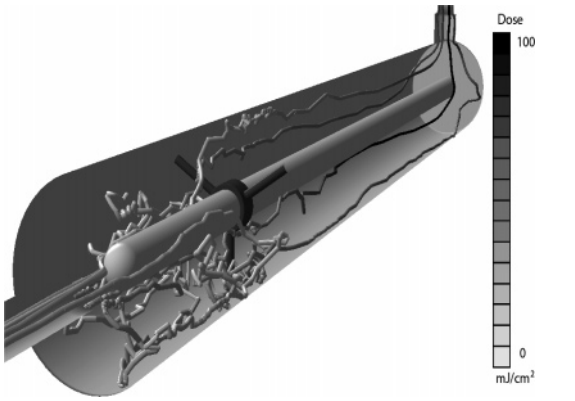

FIGURE 4. Lagrangian particles' tracks in an L-shape reactor shaded by absorbed dose.

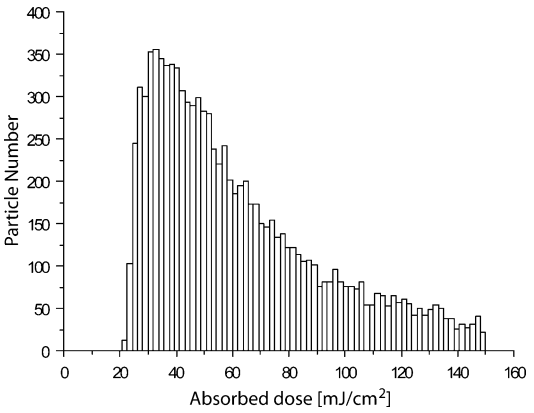

FIGURE 5. Lagrangian dose distribution, L-shape, 25 GPM with MPSS radiation model. The upper dose range was clipped at 150 mJ/cm^2 for better legibility, doses up to 270 mJ/cm^2 were reached infrequently.

4.4 Eulerian Approach for Simulating Reactor Performance. The concentration distribution of active microorganisms within the same L-shape reactor was estimated using the Eulerian method. Figure 6a shows the concentration distribution of living microorganisms within the reactor on a log scale where higher concentrations are represented by darker shades. The effect of the nonuniform fluence rate distribution on the concentration of nonreacted or living microorganisms is clearly visible. The contours of similar concentration are strongly slanted, with lower concentrations close to the lamp surface appearing earlier on the reactor axis. The contours of local reaction rates presented on a log scale in Figure 6b show similar tendencies but with a less distinct influence of the flow. This is understandable because reaction rates are a function of both the stationary fluence rate as well as the flow dependent microorganism concentration. In Figure 6b, the effect of flow recirculation (see Figure 2a) is evident at the reactor inlet near the reactor walls, where, despite low fluence rates, relatively high reaction rates are observed because of higher residence times. The average mass fractions of microorganisms at both inlet and outlet of the reactor are determined through integration to calculate the reactor's total inactivation rate, resulting in a log reduction of 2.07; 10% higher than that predicted by the Lagrangian model.

4.5 Comparison of Inactivation in Two Reactor Geometries. The influence of reactor geometry, flow rate, and

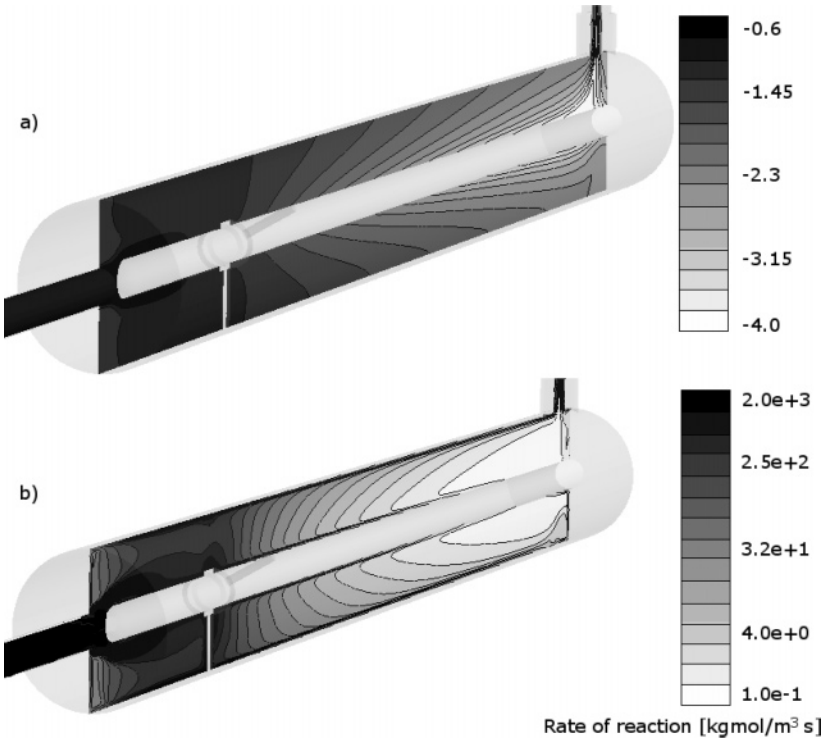

FIGURE 6. (a) Contours of microorganism concentration, mass fraction on a log scale. (b) Contours of disinfection reaction rates [kgmol/m³s] on a log scale. L-shape, 25 GPM with MPSS lamp model.

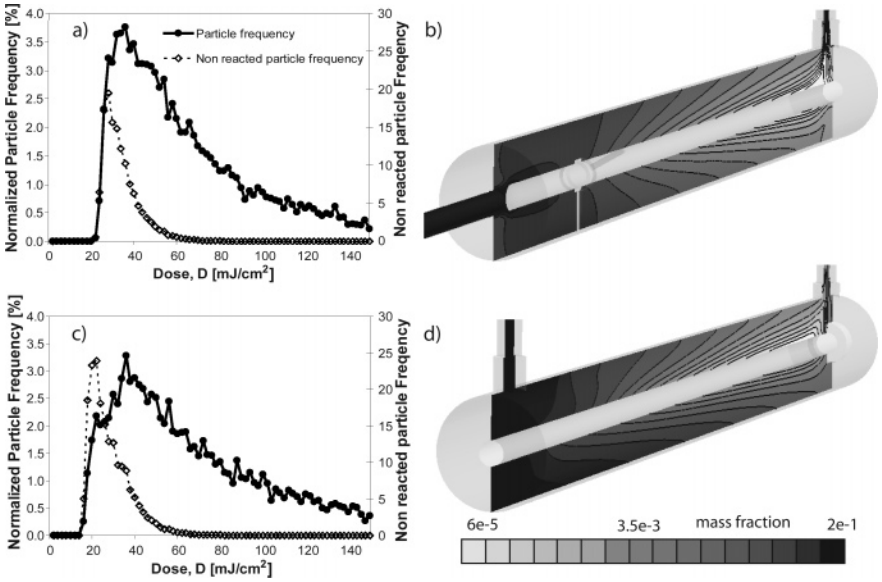

FIGURE 7. Lagrangian dose distribution (a, c) and Eulerian concentration distribution (b, d) for L- and U-shape reactor geometries. Range of Lagrangian results clipped at 150 mJ/cm² for better legibility.

radiation model on the Eulerian and Lagrangian reactor performance predictions was investigated. The Eulerian microorganism concentration and Lagrangian dose distribution for both L- and U-shape reactor geometries, using the MPSS radiation model at a UV transmissivity of 70%, are presented in Figure 7 for a mass flow rate of 25 GPM. The influence of the reactor geometry is clearly visible in the inlet region and along the lower reactor wall where higher flow speeds in the U-shape reactor (see Figure 2b) lead to lowered local rates of disinfection (Figure 7b and d). This qualitative view of microorganism concentration distribution can be helpful to identify the areas of short circuiting. This nonideal behavior is also discernible through a shoulder in the lower ranges of the Lagrangian dose distribution where some particles receive less than 20 mJ/cm² in the U-shape reactor (Figure 7c). Microorganisms in this dose range did not receive enough dose to be disinfected effectively by remaining far from the radiation source and passing through the reactor volume at a high velocity. The secondary distribution curves in Figure 7a and c, indicate the number of noninactivated microorganisms and show that the mean dose is of little importance on the reactor performance, because unreacted microorganisms affecting the log total reactor reduction only occur in significant numbers at lower doses. The distribution profile also shows the number of organisms that receive very high doses, uncovering the relatively low impact of these organisms on reactor overall performance (that is, the reactor performance is mainly determined by the microorganisms receiving low doses).

TABLE 2. Log Reduction Results over a Range of Flow Rates for the L-Shape Reactor[a]

	10 GPM		15 GPM		25 GPM		35 GPM	
	Eul.	Lagr.	Eul.	Lagr.	Eul.	Lagr.	Eul.	Lagr.
L-shape								
radial	3.10	2.71	2.31	2.04	1.50	1.36	1.12	1.07
MPSS	4.18	3.64	3.15	2.79	2.07	1.87	1.55	1.45
% difference	25.8	26.1	26.6	26.8	27.4	27.2	27.8	26.3
U-shape								
radial	2.76	2.41	2.03	1.88	1.37	1.29	1.08	1.04
MPSS	3.66	3.16	2.71	2.44	1.86	1.72	1.45	1.39
% difference	24.7	23.8	25.0	23.0	26.4	25.0	25.1	25.2

[a] Comparison of radial and MPSS lamp radiation models using both Eulerian and Lagrangian approaches. The lamp models consistently show about 26 ± 1.5% difference in log reduction.

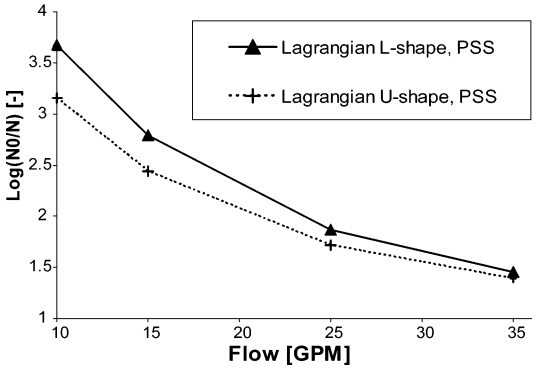

FIGURE 8. Log reduction in the L- and U-shape reactor geometries for different flow rates. Lagrangian approach with MPSS radiation at 70% UV transmittance (per cm).

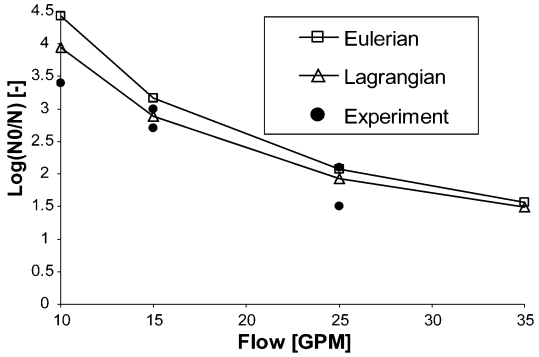

FIGURE 9. Eulerian and Lagrangian model results (MPSS radiation model with 70% UV transmissivity) compared to experimental data over a range of flow rates for a commercial L-shape reactor.

For the quantitative comparison of L- and U-shape reactors at various flow rates, the inlet flows of 10, 15, 25, and 35 GPM (6.3×10^{-4}, 9.5×10^{-4}, 15.8×10^{-4}, and 22.1×10^{-4} m^3/s, respectively) were simulated, using the MPSS radiation model at a UV transmissivity of 70%. The log reduction results for both reactor geometries using the Lagrangian approach are shown in Figure 8. Although the L-shape reactor performed better for the tested flow range, the performance difference of the L- shape and U-shape reactors was dependent on the flow rate. The differences relative to the L-shape results ranged from 14% at 10 GPM to 3% at 35 GPM. This is consistent with the notion of short circuiting occurring in the U-shape reactor. As Figure 7a and c show, reactor performance is largely defined by the microorganisms receiving lower doses. At high flow rates, the short residence time results in an overall shift to the lower dose range. Short circuiting in the U-shape reactor still occurs, but has less influence on the total log reduction levels reached. At lower flow rates, microorganisms reach higher overall doses and the L-shape reactor performs well. In the U-shape reactor, on the other hand, short circuiting still occurs and its influence on reactor performance is more pronounced. A relative performance increase of 10% for the L-shape in the target log reduction range is substantial. The fact that this performance gain is evoked by a simple change in inlet placement underlines the importance of including hydrodynamic considerations into reactor design.

To study the impact of radiation models on the reactor performance results, the L- and U-shape reactors were simulated using the infinite line source (radial) and finite line source (MPSS) radiation models. For the given reactor dimensions, where the reactor walls are only 4.45 cm from the lamp surface, the lamp models have a marked influence on the simulated reactor performance (Table 2). The radial lamp model shows a 26 ± 1.5% lower log reduction over the entire calculated range of flow rates; the same relative difference was observed for both reactor geometries. This is consistent with the noted higher UV output predicted in the near lamp region for the MPSS model (Figure 3) and demonstrates the importance of using an accurate radiation model in reactor performance simulations.

4.6 UV Reactor Model Evaluation. To experimentally verify the reactor performance models, the log reduction of a commercial annular L-shape UV-disinfection reactor was simulated (Figure 1c, dimensions in Table 1). The main details of the internal reactor geometry, including a more complex lamp holder at the inlet and a reduction ring close to the outlet, were considered in the simulation. The reactor performance was calculated, implementing the integrated CFD model by discretizing the domain with 0.7 million cells, accounting for turbulence with the realizable κ-ϵ model and applying both Lagrangian and Eulerian disinfection models.

The log reductions predicted by the Lagrangian and Eulerian methods for a range of flow rates at a transmissivity of 70% are presented in Figure 9. The transmissivity T = 0.7 and the reaction rate constant $k = 0.1$ were obtained from experimental measurements. Both modeling approaches show very similar responses regarding the influence of flow rate on the log reduction. For a flow of 10 GPM, the difference between the two methods was 11% and it decreased to about 4.5% at a flow rate of 35 GPM. Similar trends in reactor performance difference using the Eulerian and Lagrangian models were observed for the L- and U-shape geometries (explained in Section 4.5). The deviation between the Eulerian and Lagrangian methods has not been examined in depth, but possible causes are the different approaches taken by the two models. The particle trajectories, calculated by the Lagrangian method, may not cover the entire reactor domain, causing differences between the Eulerian and Lagrangian results. In addition, the uncertainties associated with the finite-rate reaction model (eddy- dissipation model used) and the assumptions made for the calculation of absorbed

energy per cell (small spherical cells) in the Eulerian model, may contribute to the deviation between the results from the two models. Both modeling results show a good agreement with the biodosimetry measurements performed for this reactor. Like most biological assays, biodosimetry has a considerable variance and not enough experimental values were available for a detailed comparison of the modeling approaches. However, the results indicate the possibility of modeling a UV reactor's performance to a close degree, knowing the geometrical specifications and operating conditions using either the Lagrangian or Eulerian approaches.

The information gained from the two modeling approaches is complimentary rather than overlapping; while the Lagrangian method provides estimates of the UV-dose distribution and the particle tracks visualize flows patterns, the Eulerian approach shows the concentration distribution and local reaction rates. The combined information can be used to predict and monitor reactor performance levels and to enhance the reactor designs. At a higher computational cost, the Eulerian model delivers a more conclusive image of the local disinfection rates within the reactor volume. More importantly, this model can be extended to UV-based advanced oxidation processes, which involve additional volumetric reactions, by including further reaction steps. Even though costly and time-consuming construction of intermediate prototypes can be reduced through the use of UV reactor simulations, complementary experiments remain necessary to verify reactor performance for the final UV reactor designs.

Symbols

C concentration of microorganisms [mol/L]

C_μ empirical coefficient, mixing length model [unitless]

D dose [mJ/cm^2]

D_1 diameter of the inlet tube [cm]

E fluence rate [mW/cm^2]

k inactivation rate constant [cm^2/mJ]

L_1 length of inlet tube [cm]

L_2 length of lamp arc [cm]

l_i distance from lamp point to current point (MPSS) [cm]

N organism concentration [PFU/mL]

N_0 initial organism concentration [PFU/mL]

n number of point sources (MPSS model) [unitless]

P germicidal lamp output (254 nm) per cm [W/cm]

Q flow rate [m^3/s]

r radial distance from lamp [cm]

r_L radius of lamp sleeve [cm]

T transmissivity of the fluid [cm^{-1}]

t time [s]

z axial distance on lamp [cm]

Greek Letters

α_i fraction of particles receiving dose D_i

ϵ turbulent energy dissipation rate

κ turbulent kinetic energy

μ_t turbulent viscosity

μ fluid viscosity [kg/m s]

σ_w absorption coefficient of fluid [cm^{-1}]

Literature Cited

(1) Pirnie, M.; Linden, K. G.; Malley, J. P. *Ultraviolet Disinfection Guidance Manual, Draft*; U.S. Environmental Protection Agency: Washington, DC, 2003.

(2) Schoenen, D.; Kolch, A.; Gebel, J. Influence of geomtetrical parameters in different irradiation vessels on UV disinfection rate. *Int. J. Hyg. Environ. Med.* **1993**, *194,* 313−320.

(3) Chiu, K.; Lyn, D. A.; Blatchley, E. R. Integrate UV disinfection model based on particle tracking. *J. Environ. Eng.* **1999**, 7−16.

(4) Pareek, V. K.; Cox, S. J.; Brungs, M. P.; Young, B.; Adesina, A. A. Computational fluid dynamic (CFD) simulation of a pilot-scale annular bubble column photocatalytic reactor. *Chem. Eng. Sci.* **2003**, *58,* 859−865.

(5) Bakker, A.; Haidari, A. H.; Marshall, E. M. Design reactors via CFD. *CEP Mag.* **2001**, *December,* 30−39.

(6) Unluturk, S. K.;Arastoopour, H.; Koutchma, T. Modeling of UV dose distribution in a thin-film UV reactor for processing of apple cider. *J. Food Eng.* **2004**, *65,* 125−136.

(7) Lyn, D. A.; Chiu, K.; Blatchley, E. R., I. Numerical modeling of flow and disinfection in UV disinfection channels. *J. Environ. Eng. (Reston, VA, U. S.)* **1999**, *125,* 17−26.

(8) Kamimura, M.; Furukawa, S.; Hirotsuji, J. Development of a simulator for Ozone/UV reactor based on CFD analysis. *Water Sci. Technol.* **2002**, *46,* 13−19.

(9) Lawryshyn, Y. A.; Lu, D. UV Reactor Design. *Water Conditioning Purif. Mag.* **1999**, *41.2,* 13−19.

(10) Lawryshyn, Y. A.; Cairns, B. UV disinfection of water: the need for UV reactor validation. *Water Sci. Technol.* **2003**, *3.4,* 293−300.

(11) Sozzi, A.; Taghipour, F. Experimental Investigation of Flow Field in Annular UV Reactors Using PIV. *Ind. Eng. Chem. Res.* **2005**, *44,* 9979−9988.

(12) Blatchley, E. R. Numerical modelling of UV intensity: Application to collimated-beam reactors and continuous flow systems. *Water Res.* **1997**, *31,* 2205−2218.

(13) Liu, D.; Ducoste, J.; Jin, S.; Linden, K. Evaluation of alternative fluence rate distribution models. *J. Water Supply: Res. Technol.−AQUA* **2004**, *53.6,* 391−408.

(14) Taghipour, F. Ultraviolet and ionizing radiation for microorganism inactivation. *Water Res.* **2004**, *38,* 3940−3948.

(15) Bolton, J. R. Calculation of ultraviolet fluence rate distributions in an annular reactor: Significance of refraction and reflection. *Water Res.* **2000**, *34,* 3315−3324.

(16) Scheible, O. K.; McGrath, J. A. *Generic verification protocol for high- rate, wet-weather flow disinfection applications*; Technical Report; U.S. Environmental Protection Agency: Washington, DC, 2000.

(17) Mofidi, A. A.; Coffey, B. M.; Green, J. F.; Chou, C. I. *Investigation of Ultraviolet Light Disinfection*; Technical Report; Metropolitan Water District of Southern California: Los Angeles, CA, 2002.

(18) Mulkey, L. A. ETV Joint verification statement, UV disinfection of secondary effluent system by Suntec Inc.; Technical Report; U.S. Environmental Protection Agency, Environmental Technology Verifcation Program; Washington, DC, 2003

(19) *Fluent User Guide: Chapter 19. Discrete phase models*; Fluent Inc.: Lebanon, NH, 2004.

(20) *Fluent User Guide: Chapter 13. Modeling species transport and finite-rate chemistry*; Fluent Inc: Lebanon, NH, 2004.

(21) Elyasi, S.; Taghipour, F. Simulation of a UV Photoreactor in an Eulerian Framework Governed by Complex Deactivation Rate of Microorganisms. In *Proceedings of Third International Congress on Ultraviolet Technologies*, Whistler, BC, May 24-27, 2005.

(22) *Standard Methods for the Examination of Water and Wastewater*, 18th ed.; American Public Health Association: Washington, DC, 1998.

Received for review May 28, 2005. Revised manuscript received November 9, 2005. Accepted November 14, 2005.

ES051006X